Numerical and Experimental Characterization of a New Reduced-Height CALORRE Differential Calorimeter for CALOR-I Irradiation in MITR

A. Volte, S. Hauptman, D. Carpenter, M. Carette, A. Lyoussi, G. Kohse, C. Reynard-Carette

Numerical and experimental characterization of a new reduced-height CALORRE differential calorimeter for CALOR-I Irradiation in MITR

A. Volte, S. Hauptman, D. Carpenter, M. Carette, A. Lyoussi, G. Kohse, C. Reynard-Carette

***Abstract*— This paper presents the preliminary characterization of a new reduced-height CALORRE differential calorimeter designed by Aix Marseille University and fabricated in order to be tested and qualified under irradiation in the MITR experimental reactor within the framework of the CALOR-I program. The paper begins by focusing on the preparation of the irradiation campaign, providing a concise description of the MITR core, the water loop facility, and the newly fabricated differential calorimeter. Then, this work summarizes neutronic calculations performed for the CALORRE differential calorimeter to provide data for the irradiation campaign. MCNP calculation code was used to predict the neutron and gamma flux spectra, and total nuclear heating rate to the components of the calorimeter in a variety of positions. The MCNP model parameters and methodology are detailed and results are used to perform 3-D thermal modelling. Estimation of the response of the calorimeter calculated under real conditions considering local heat sources determined by the NRL of the MIT using MCNP code is given. Next, the paper presents the experimental characterization conducted under laboratory conditions. This section includes a detailed presentation of the updated experimental set-up and the key metrological characteristics of the sensor response obtained from the experimental results. In conclusion, the paper offers some final remarks and prospects to realize the irradiation campaign successfully.**

***Index Terms*— Calorimeter, Nuclear Heating Rate, On-line Measurements, Calibration, Irradiation campaign, Neutronics.**

I. Introduction

Knowledge of the properties of materials in nuclear environments is crucial to design new systems and major facilities whether for nuclear fission or fusion purposes. To improve the understanding of phenomena that occur in materials in such harsh environments particularly in terms of nuclear flux, temperature, nuclear adsorbed dose rate, ageing, activation and thus to have accurate data, numerical and experimental studies are required. The research reactors corresponding to Material Testing Reactors (MTRs) are very valuable to conduct this kind of work as they produce relevant conditions including high neutron and gamma fluxes, high nuclear absorbed dose rate also known as nuclear heating rate, as well as strong displacement per atom and because they allow a wide capability of dedicated experiments on nuclear, mechanical, chemical and thermal aspects (damage, corrosion, fission product release…) for materials and nuclear fuels. A new MTR is under construction at the CEA Cadarache Center in the south of France. It is called Jules Horowitz reactor (JHR). This new research reactor with a 100 MW_{th} nominal thermal power will provide high-level research and development possibilities in Europe thanks to a high fast neutron flux of $5.5x10^{14}$ $n.cm^{-2}.s^{-1}$ (from 1 MeV) leading to high accelerated aging (up to 16 $dpa.year^{-1}$) and a high nuclear absorbed dose rate (up to 20 $W.g^{-1}$ in aluminum). Since 2009, Aix-Marseille University (AMU) and the CEA (within the framework of the joint laboratory LIMMEX - Laboratory for Instrumentation and Measurement in Extreme Environments) have been carrying out research works to develop innovative instrumentation and advanced measurement methods for future online measurements of key parameters inside the irradiation channels of the JHR [1, 2]. One targeted key parameter corresponds to the nuclear heating rate quantified by calorimeter [3-10]. A comprehensive approach has been developed to design and qualify several calorimeter prototypes. This approach includes sensor design and behavior prediction by 3-D numerical simulations, parametrical characterization of the sensor response in terms of metrological performances (reached temperature, response time, linearity, sensitivity, nuclear heating rate range) under laboratory conditions without nuclear radiation, out-of-pile calibration by using specific benches (transient or steady method) and sensor qualification by means of irradiation campaigns inside international research reactor. This approach led to promising results regarding the new calorimeter patented in 2015 and called CALORRE [5-10]. This prototype is a heat-flow differential calorimeter composed of two superimposed compact calorimetric cells with a specific geometry allowing heat transfer in both radial and azimuthal directions to significantly reduce axial heat losses. A first prototype was tested successfully for the first time in November 2015 in the MARIA reactor at 24 MW with a multi-calorimeters device [9, 10] and a new more compact prototype (88.5 mm against 222.5 mm) was defined by AMU [10] within the framework of the CALOR-I research program involving the Nuclear Reactor Laboratory of the MIT and the CEA (CALOR-I: compact-CALORimeter Irradiations inside the MIT Research

This paper was submitted on October 1, 2023.
"The CALOR-I project leading to this publication has received funding from the Excellence Initiative of Aix-Marseille University - A*Midex, a French "Investissements d'Avenir" programme", AMX-19-IET-013.
A. Volte, M. Carette, C. Reynard-Carette are with Aix Marseille Univ, Université de Toulon, CNRS, IM2NP, Marseille, France (e-mail: adrien.volte@im2np.fr, michel.carette@univ-amu.fr, christelle.carette@univ-amu.fr).
A. Lyoussi, is with CEA/DES/IRESNE/DER, Section of Experimental Physics, Safety Tests and Instrumentation, Cadarache, F-13108, Saint Paul-lez-Durance, France (e-mail: abdallah.lyoussi@cea.fr).
S. Hauptman, D. Carpenter and G. Kohse is with Massachusetts Institute of Technology, Nuclear Reactor Laboratory, Cambridge, Massachusetts, USA (e-mail: hauptman@mit.edu, david_c@mit.edu, kohse@mit.edu).

Reactor, program funded by A*Midex Foundation, 2020-2024).

Before a future irradiation campaign in the MIT reactor loop to qualify this reduced-size CALORRE prototype, the new aims and steps of this program are the estimation of the nuclear heating rate in this prototype inside the MITR water loop by Monte Carlo calculations [11], the prediction of the sensor response by considering these ray-matter interaction results, and finally the experimental study of the fabricated prototype by imposing specific laboratory conditions and protocols to obtain its calibration curves. This paper will focus especially on these steps and the associated results.

The first part of the paper will detail the future MITR water loop environment and the new reduced-sized calorimeter.

The second part will deal with the 3-D numerical work under real conditions from the determination of the local nuclear heating rate in all the components of the CALORRE calorimetric cells using a MITR core model and with MCNP calculations. An estimation of the energy deposition with a calculation of the energy deposition due to prompt gammas, neutrons and a preliminary evaluation of the energy deposition of delayed gammas with an empirical formula was performed. These initial calculations aimed to estimate with safety margins the nuclear absorbed dose rate. Then, 3-D thermal simulations of the calorimeter were realized by coupling these nuclear heating rate results with COMSOL Multiphysics to study the thermal response. This enabled the sensor to be designed on the criterion of the maximum temperature, the temperature of the external envelope and the sensitivity under real conditions.

The third part will give and discuss the metrological characteristics of the prototype obtained experimentally under calibration protocol and their comparison with those of other calorimeters.

II. PREPARATION OF AN IRRADIATION CAMPAIGN INSIDE THE MIT REACTOR

The irradiation campaign inside the MITR has three primary objectives: mapping for the first time the nuclear heating rate within the MITR core using two sensors (the CALORRE differential calorimeter and a commercial sensor), studying a new compact CALORRE prototype for the in-core water loop through two measurement methods, and assessing the impact of various conditions (such as convection intensity and reactor power). The following sub-sections will provide a brief overview of the MIT reactor core and water loop facility, followed by the introduction of the new calorimeter prototype.

A. The MITR core

The Massachusetts Institute of Technology (MIT) Research Reactor (MITR), is a light-water cooled and moderated tank-type reactor, licensed for operation up to 6 MW_{th}. A horizontal cross-section of the core is shown in Figure 1, where A1, A3, and B3 are the three designated experiment positions, and the remaining twenty-four spots contain rhombic elements with plate-type fuel [12].

The MITR can be started up to full power in as little as a few hours and will reach thermal equilibrium across all systems after a few days of operation. Power changes for irradiations are not limited for any decrease in power, but cannot increase by more than 1.0 MW in a single step, and must have at least 5 min of soak time between steps.

The control devices for MITR consist of six Boron-10 impregnated stainless-steel shim blades around the periphery of the core, shown in dark blue in Figure 1, and a single Cadmium wrapped regulating rod located in a corner housing. The symmetry of control devices provides a very steady radial flux profile during the course of operation. The axial profile is influenced by the withdrawal of the shim blades, leading to the largest flux peaking being observed at the very beginning of cycle and flattening of the profile occurring in response to blade withdrawal to compensate for neutron poison build-up within the first few days of start-up.

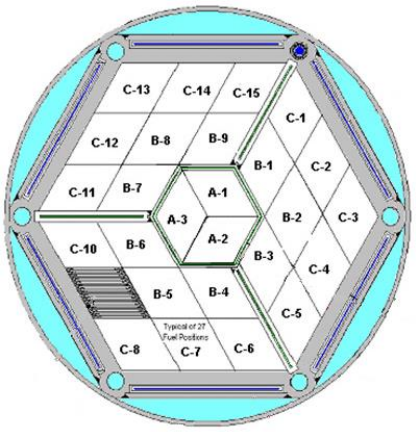

Fig. 1. Horizontal cross section diagram of MITR core with element positions labelled and reactivity control devices shown in dark blue. Position C-9 shows the reference orientation of the fuel plates.

B. MITR Water Loop Facility

Out of the three core positions approved for installed experiment facilities, one is designed to accommodate the High Temperature Water Loop (HTWL); an isolated circulating loop independent from the reactor process systems, capable of matching PWR or BWR water chemistry, temperature, and pressure conditions for the materials and components undergoing irradiation [13].

The loop flows through an inlet line down to the experimental thimble installed in the active core region, through a down comer, around the sample of interest, and into a return line. The inlet and return lines penetrate through a plug in the reactor top lid and allow for instrumentation and control systems to remain accessible to personnel working on the reactor top. A cutaway schematic of the core tank section of the HTWL is shown in Figure 2.

Due to the geometry of the reactor lid penetrations, the B3 core position is the only possible location for the HTWL to be installed. The HTWL system allows for more precise control of the irradiation environment temperature compared to the dry facilities that must be used in the remaining two core experiment positions. This temperature control capability is the reason the HTWL was selected for the CALOR-I campaign.

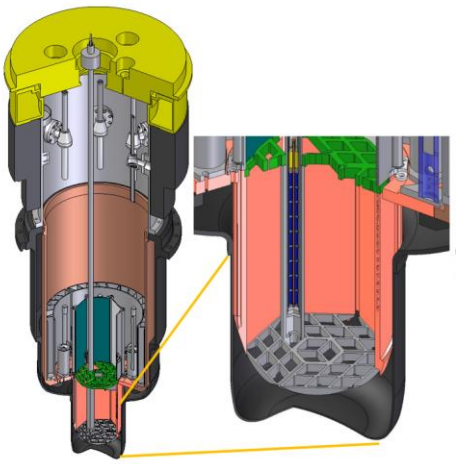

Fig. 2. Diagram of installed HTWL facility in B3 position. Fuel elements are omitted for clarity.

C. *The new differential calorimeter prototype*

As previously mentioned, the design of the differential calorimeter prototype (CALORRE type) was based on previous irradiation campaigns, recent research results, data from six additional calorimetric cells, and the nuclear heating rate predicted in MITR [11]. The prototype composed of two superimposed calorimetric cells (sample and reference cells) was rigorously defined using 3-D numerical thermal simulations, with the aim of removing thermal contact resistances, simplifying component assembly and integration, and limiting the overall height of the calorimeter [10]. To achieve the objectives, a modified configuration that featured a reduced-height calorimetric cell, measuring 11.55 mm in height was defined.

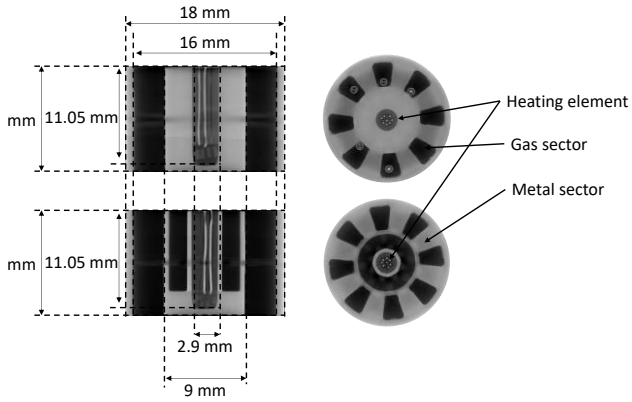

Fig. 3. 3-D microtomography of each fabricated calorimetric cell (left-hand section) and horizontal fin (right-hand section) of the sample cell (upper part) and reference cell (lower part) respectively.

Each new calorimetric cell comprises an arrangement of stainless-steel half-horizontal fins, consisting of 8 metal sectors and 8 empty sectors, each with an equal angle of 22.5°, as shown in Figure 3. Additionally, the vertical-fin height was increased to 31.55 mm, compared with 11.55 mm previously. The vertical-fin is now used as an envelope. In particular for the sample calorimetric cell, the sample and head structure were built into a single stainless-steel block (cf. Figure 3) for the sample cell, making the assembly easier and avoiding thermal contact resistances. The vertical fins of both the sample and reference cells were welded together, as illustrated in Figure 4, which eliminated the need for spacers and resulted in a watertight unified calorimeter structure filled with di-nitrogen.

Figure 4 shows an overview of the compact CALORRE differential calorimeter designed for MITR irradiation. This calorimeter has an 18 mm inter-cell spacing, giving an inter-sample spacing of 29.55 mm. This significantly reduces the 95 mm spacing used during the MARIA campaign [9, 10].

Furthermore, to do out-of-pile calibration and to apply several measurement methods in reactor, each cell includes a heating element in its center. These central heating elements are connected in a 4-wire configuration using Nickel-Chromium wires. The resistance of the sample cell heating element is equal to 2.21 Ohm as against 2.02 Ohm for that of the reference cell. This setup enables precise control of the electrical power during calibration, ensuring it accurately represents the targeted nuclear heating rate range and to take variations in resistance depending on conditions, such as temperature into account. Each cell is equipped with two K-type thermocouples placed at specific locations, consistent with previous configurations, for temperature measurements. The thermocouples and the connection wiring for the 4-wire heater will be carefully routed through the interior of the calorimeter, extending outward from the top (cf. Figure 4). These connections will then connect back to the measurement system outside of the core. A total of 9 cables (4 cables for thermocouples and 5 cables for the 2 heating elements), each with a length of 20 meters, need to be pulled up.

The precise positioning of the calorimeter within the water loop autoclave will be facilitated by a dedicated device. This device is overseen and controlled by MITR controllers, with corresponding indications provided [13].

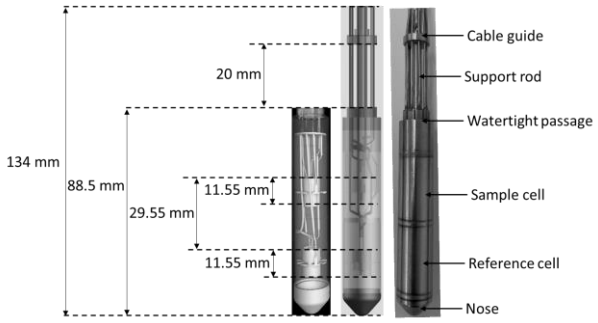

Fig. 4. 3-D microtomography (left-hand section), scheme (middle section) and picture (right-hand section) of the CALORRE differential calorimeter.

The calorimeter is structured from bottom to top and comprises the following components: nose, reference cell, sample cell, watertight passage, support rod, and cable guide. The total height, measured from the base of the nose to the top of the support rod, is 134 mm. Notably, the distance from the bottom of the nose to the top of the watertight passage is only 88.5 mm, a significant reduction compared to the CALORRE-MARIA, CARMEN and CALMOS differential calorimeters, which measure 222.5 mm. Despite these changes, the outside

diameter remains constant at 18 mm (with a vertical-fin thickness of 1 mm).

III. 3-D NUMERICAL CALCULATIONS UNDER REAL CONDITIONS

A. MCNP Model Parameters and Methodology

Assumptions were made to simplify the neutronic modeling while preserving the accuracy of the results. Figure 5 shows the comparison between the mechanical model and the visualization of the geometry in the MCNP input deck. The smaller instrumentation masses of the wires and thermocouples were neglected from the neutronic input deck as they are unlikely to impact the tally results of the larger components. The fixtures and structural supports holding the calorimeter itself in place in the HTWL were also neglected due to their distance from the region of interest.

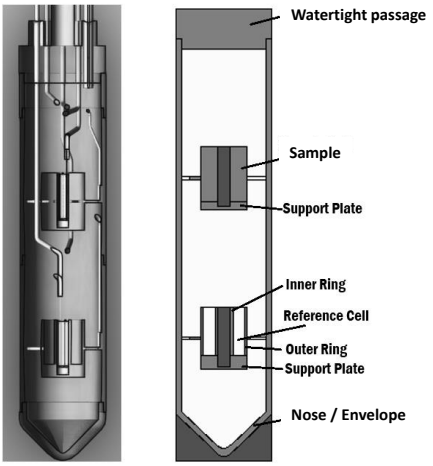

Fig. 5. CAD drawing (left-hand section), converted into MCNP input geometry (right-hand section) with labels corresponding to component designations for nuclear heating rate results.

The shape of the calorimeter and more specifically the displacement of the water volume within the HTWL was preserved (cf. Figure 6).

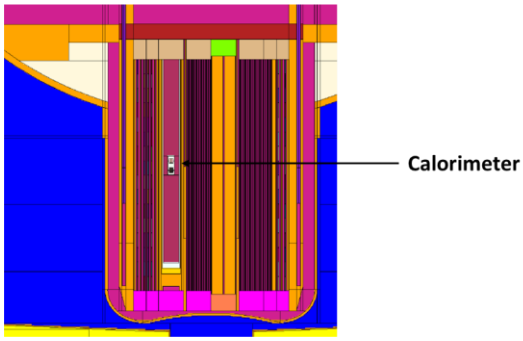

Fig. 6. MCNP model diagram with the sensor in the core.

The heating calculations were performed with MCNP5 v1.60 using ENDF-VII nuclear data libraries [14, 15]. Comparison checks were done with MCNP6.2 using the same data resources to confirm agreement and compare different tally methodologies. Electron heating contributions were counted as heating deposited locally with photon interactions in the model. Separated electron and photon heating component tallies were performed with MCNP6 to verify agreement and justify the simplified physics treatment settings. For a coupled neutron-photon problem, MCNP5 was selected due to the reduced computational runtime. Equivalent problems were run in both versions and MCNP5 produced results with improved statistics and reduced computational time required compared to MCNP6. The settings and average CPU time requirements are summarized in Table I. A comparison of the total nuclear heating rate for identical capsule position at the fuel centerline, run in both versions is also listed for the averaged fin values and sample material.

TABLE I
COMPUTATIONAL RUNTIME AND TOTAL NUCLEAR HEATING RATE COMPARISON FOR MCNP VERSIONS

Problem Settings	MCNP5 1.6	MCNP6.2
Cycles	820	220
Histories	800,000	400,000
Average CPU runtime [min]	11,469	36,311
Total Nuclear Heating Rate [W.g^{-1}] – Fin Average	1.92	1.91
Total Nuclear Heating Rate [W.g^{-1}] - Sample	1.86	1.85

MCNP is not capable of tallying directly the heating contribution due to delayed gamma production, which is a significant proportion of the nuclear heat deposited in the materials. For this reason, the F6 neutron and prompt gamma energy deposition tallies were used in order to separate the heating contributions.

In the literature, two tendencies are used to determine the nuclear heating rate. The first approach is to initially take into account the neutron heating rate and the prompt gamma heating rate without the calculation of the contribution of the delayed gamma [4, 16, 17]. The second approach is to add this contribution with numerical calculations [18, 19]. The results show that delayed photons make a significant contribution to total energy deposition and are therefore important for thermal design. However, this method requires more resources and precise knowledge of the state of the fuel. For this reason, an intermediate method, using an empirical formula, was chosen to begin with, as the contribution of the delayed photons to the total energy deposition is ~20% for a graphite sample in the literature.

The differential calorimeter prototype was fabricated using stainless steel 316L (austenitic stainless steel) with a low cobalt level (0.04%) except for the heating elements. It was chosen to reduce energy deposition from the radioactive decay of Co-60. However, NAA is in progress to accurately measure the composition of stainless steel.

The calculation of delayed gamma heating can be found using Eq. 1 where the delayed gamma component can be calculated with an empirical conversion factor of 1.53 [20]. This empirical method was chosen to overestimate the energy deposition.

$$\gamma_{total} = \gamma_{prompt} + \gamma_{delayed} = 1.53 * \gamma_{prompt} \quad (1)$$

The total nuclear heating rate can then be calculated by adding the neutron and total prompt gamma contributions. The energy spectrum of the prompt gamma flux surrounding the calorimeter exterior is shown in Figure 7.

Each problem was run with 800 active cycles and 800,000 neutron histories per cycle to obtain tally statistics with low uncertainties, particularly for the fin geometries (horizontal and vertical fins) which are quite thin. The CALORRE calorimeter components are relatively small, but it was important to obtain distinct nuclear heating rates for each component to provide to the thermal simulations. This required more simulation time to converge with acceptable uncertainty margins. Additional random seeds were used and the resulting tallies merged for further variance reduction.

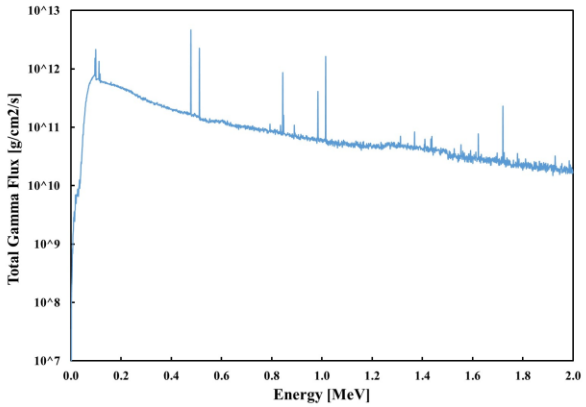

Fig. 7. Photon spectrum surrounding the calorimeter capsule.

All tally results were normalized to a reactor power of 6.0 MW. Measurements during the irradiation campaign may be performed at various power levels but the correction to lower power is linearly proportional and does not require separate simulation results. Nuclear heating rates were tallied for a variety of core axial locations in order to obtain a detailed map of predicted values as a function of calorimeter position (cf. Figure 8).

TABLE II
TOTAL NUCLEAR HEATING RATES FOR CALORRE COMPONENTS OBTAINED BY MCNP MODELLING

COMPONENT	MATERIAL	TOTAL NUCLEAR HEATING RATE [W/g]
Lower Heater	Alumina	1.80
Upper Heater	Alumina	1.76
Lower Support Plate	SS316L	1.97
Ref Cell Inner Ring	SS316L	1.99
Ref Cell Outer Ring	SS316L	1.99
Upper Support Plate	SS316L	1.95
Sample Cell	SS316L	1.91
Lower Fin (Avg)	SS316L	1.98
Upper Fin (Avg)	SS316L	1.95
Nose / Envelope	SS316L	2.00
Watertight passage	SS316L	1.90

A set of nuclear heating rates for each component is given in Table II. It corresponds to the problem run where the calorimeter was placed with the centerline of the sample cell fins at the peak flux location, approximately 5 cm below the fuel centerline. The total nuclear heating rates across all non-fin SS316L components and positions for the statistical combination of tallies, ranged from 1.59 ± 0.02 $W.g^{-1}$ to 2.01 ± 0.02 $W.g^{-1}$.

Figure 8 shows the nuclear heating rate of the sample versus the axial position of the nose cone plane to observe the nuclear heating rate profile expected in the water loop.

The axial positions were spaced apart such that there would be data points pairing the sample cell and reference cell at the same location.

This provided a baseline prediction for a correction factor to adjust for the axial flux gradient between the two cells at different potential measurement locations.

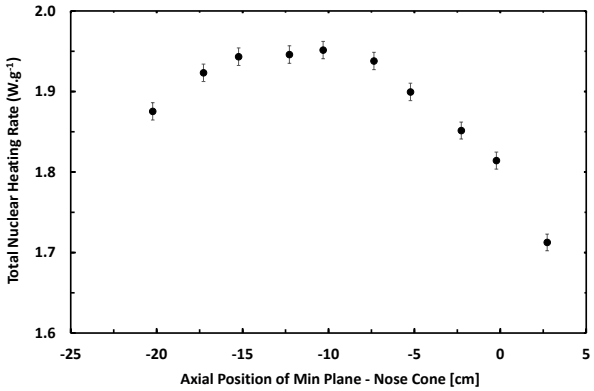

Fig. 8. Axial nuclear heating rate profile of the sample versus the axial position of the nose cone plane.

B. 3-D Numerical thermal calculations

The performance analysis of the new compact differential calorimeter response was conducted under irradiation conditions by 3-D simulations for a simplified geometry focusing on the two calorimetric cells, the nose, the watertight passage, the support rod, and the cable guide. Cables and thermocouples were not included in the analysis.

To carry out this study, these 3-D numerical simulations use a validated thermal model for the steady state [9, 10]. The thermal model was solved using COMSOL Multiphysics and encompasses heat conduction transfers, taking the temperature-dependent thermal conductivity of stainless steel (experimentally measured up to 400 °C thanks to a Hot Disk instrument) and di-nitrogen into account. In addition, radiative heat transfers were included, assuming a constant emissivity of 0.25 for stainless steel walls (internal envelope surface and external head surface) [3-4, 10]. Local heat sources were used for each calorimeter position (10 specific positions (see Figure 9)). These local heat sources (uniform value for each region depending on the region of the calorimeter) were determined by considering the nuclear heating rate results obtained thanks to MCNP code for each calorimeter component and the material density of each component.

Although it is not mentioned in Table II, the energy deposition in the gas in the reference cell (and in the calorimeter assembly) was calculated (without specifically taking into

account the decay of C-14 produced with the reaction N-14(n,p)C-14) and its impact on the thermal response is negligible, for example, the thermal heat source corresponding to the gas in the reference cell is 2.15 10^{-3} W.cm^{-3} for the nuclear heating peak compared with 14.75 W.cm^{-3} for the heat source corresponding to the sample in the sample cell.

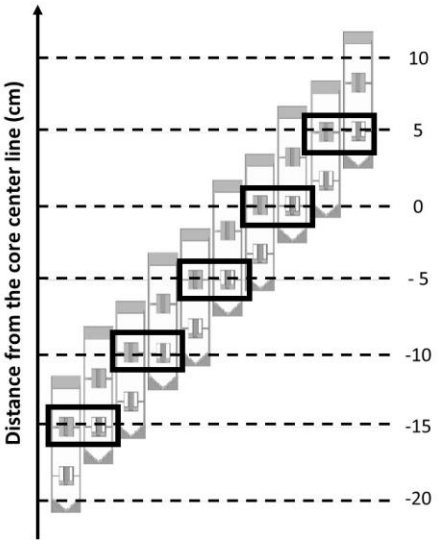

Fig. 9. Schematic of the different axial positions simulated with MCNP and the different displacements for the 10 axial positions inside the MITR water loop.

The positions were preliminary fixed to map the entire water loop and to have 5 positions where the sample and reference cells were at the same axial position (black square in Figure 9).

The external surfaces of the calorimeter were subjected to convective boundary conditions, assuming turbulent fluid flow with a heat transfer coefficient of 10000 W.m^{-2}.K^{-1} and a coolant fluid temperature of 50 °C.

This coolant fluid temperature will be the first applied in the MITR water loop. The temperature can be set in the in-core water loop. We will start with a fluid temperature of 50 °C and plan to change this value during the irradiation campaign, after which further numerical calculations will involve changing the fluid temperature. For the heat transfer coefficient, previous numerical simulations have been carried out modifying this value and the impact of h is negligible from 5000 W.m^{-2}.K^{-1} for the maximum temperature and 10000 W.m^{-2}.K^{-1} for the external wall temperature [10]. The fluid speed can also be modified and fixed in the internal water loop. The aim during the irradiation campaign will be to set a higher velocity value than that used in the 3-D calculations so as not to influence the response of the calorimeter.

Firstly, the maximum temperature inside the calorimeter and the maximum temperature at the outer wall of the envelope are studied to ensure that melting temperatures are not reached, or even that there is no risk of boiling [10] for a reactor thermal power of 6 MW_{th}. Figure 10 shows the results as a function of the axial position of the nose cone plane. The maximum temperature does not exceed 297.5 °C and the maximum temperature at the outer wall of the envelope is 59.5 °C at -10.31 cm to the core center line.

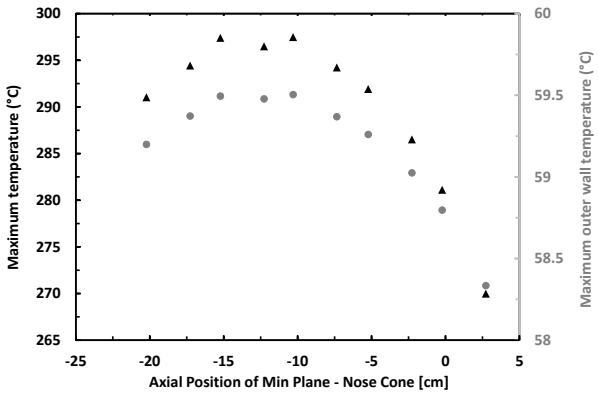

Fig. 10. Maximum temperature of the calorimeter (dark triangle) and its maximum outer wall temperature (grey circle) versus the axial position of the nose cone plane obtained numerically (h=10000 W.°C^{-1}.m^{-2} and T_f=50 °C and reactor power of 6 MW_{th}).

Then, the 3-D numerical response of each calorimetric cell is obtained. The response of the sample cell is defined by the temperature difference ($\Delta T_{sample\ cell}$) between the temperature measured close to the external surface of the sample cell head ($T_{hot\ sample\ cell}$) and the temperature measured near the internal surface of the sample cell vertical-fin at 180° ($T_{cold\ sample\ cell}$) and that of the reference cell is defined by the temperature difference ($\Delta T_{reference\ cell}$) between the temperature measured close to the external surface of the reference cell head ($T_{hot\ reference\ cell}$) and the temperature measured near the internal surface of the reference cell vertical-fin at 180° ($T_{cold\ reference\ cell}$).

These responses were calculated as a function of the axial position of the nose cone plane. These results are presented in Figure 11.

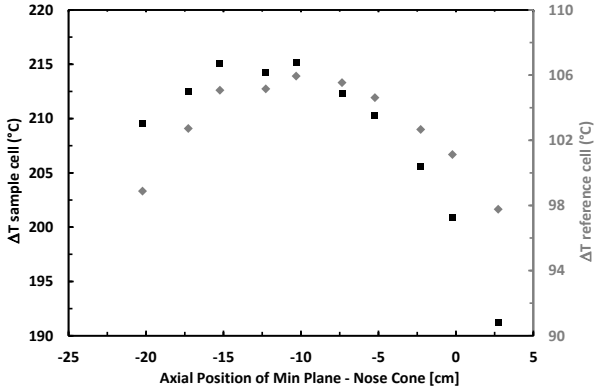

Fig. 11. 3-D numerical response of the sample cell (dark square) and that of the reference cell (grey diamond) versus the axial position of the nose cone plane (h=10000 W.°C^{-1}.m^{-2} and T_f=50 °C, reactor power of 6 MW_{th}).

As expected, for the same axial position, the temperature difference obtained under irradiation conditions is greater for the sample cell than the reference cell due to the mass of the sample which results in a higher energy deposition. For instance, at -10.31 cm which is the nuclear heating rate peak, $\Delta T_{sample\ cell}$ = 215.2 °C as against $\Delta T_{reference\ cell}$ =106 °C. These important temperature differences, particularly for the sample cell, could have an impact on the mechanical aspects of the calorimeter. The thermal expansion was not considered in 3-D

numerical thermal simulations that do not include mechanical effects. Nevertheless, the thermal expansion was measured experimentally and is equal to ~1.5 10^{-5} $°C^{-1}$ (for a temperature range from 50 °C to 250 °C). As a result, with a temperature difference of 200 °C and for a length of 1 cm (for the sample cell), the induced length variation will be equal to 30 µm (a 0.3% variation) that can be neglected at a first approach.

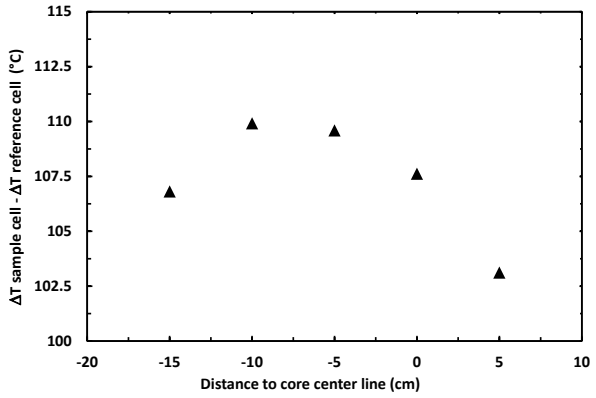

Fig. 12. 3-D numerical response of CALORRE differential calorimeter as a function of the distance to the core center line (h=10000 $W.°C^{-1}.m^{-2}$ and T_f=50 °C, reactor power of 6 MW_{th}).

Finally, the numerical calorimeter response is determined. It corresponds to the difference of the two temperature differences for the two cells located at the same axial position ($\Delta\Delta T=\Delta T_{sample\ cell} - \Delta T_{reference\ cell}$). This calorimeter response versus the distance to the core center line for a reactor power of 6 MW_{th} is presented in Figure 12. The obtained response validates the ability of the new calorimeter prototype to measure the peak nuclear heating rate, which reaches approximately 1.94 $W.g^{-1}$ at 6 MW_{th} for a stainless steel sample with a sensor sensitivity of ~56.7 $°C.g.W^{-1}$.

The coupling of MCNP and COMSOL is new for the CALORRE calorimeter. These results allow more accurate prediction of the thermal response of the CALORRE calorimeter. The response ($\Delta\Delta T=\Delta T_{sample\ cell} - \Delta T_{reference\ cell}$) is sufficiently significant to fully map the channel B3. Moreover, a quite constant level was identified between -10 and -15 cm to the core center line to perform measurement with and without displacement (cf. Figure 8 and Figure 12).

IV. Experimental Characterization under Laboratory Conditions

This section is dedicated to the experimental characterization of the fabricated new compact CALORRE differential calorimeter previously detailed in Section II.C under laboratory conditions from the updated experimental set-up to the metrological performances of the sensor. Its metrological characteristics will be compared to those obtained especially for a previous calorimetric cell having the same configuration in terms of dimensions, horizontal fin geometry, and material structure but with a sample in duralumin (non-mono-block structure) and studied individually (not mounted in a differential calorimeter assembly). This configuration corresponds to the configuration N°6 detailed in [10].

A. The experimental set-up

The previous experimental set-up was slightly modified because it was initially developed for studying an individual calorimetric cell under laboratory conditions instead of two in the case of a differential calorimeter and for lower lengths of cables [8-10]. This adapted set-up is shown in Figure 13.

This new experimental set-up is composed of: a power supply (Rhode & Schwarz NGP822, 400 W), an acquisition system (KEYSIGHT, 34972A), a computer, 2 precision resistances (a high accuracy burster 0.1 Ohm, 1240-0.1), and a thermostatic bath (ISOTECH type, parallel tube liquid bath 945). The power supply type was chosen to have sufficient power due to the increased total line resistance for each heating element (approximately 12 Ohm for the sample cell and 13.5 Ohm for the reference cell) and to be able to calibrate simultaneously the two calorimetric cells.

A total of 11 quantities are measured versus time using the acquisition system with a sampling time of 10 seconds: Hot temperature of the sample cell, Cold temperature of the sample cell, Hot temperature of the reference cell, Cold temperature of the reference cell, Voltage at heating element terminals of the sample cell, Voltage at heating element terminals of the reference cell, Voltage at the precision resistance mounted in series with the heating element of the sample cell, Voltage at precision resistance mounted in series with the heating element of the reference cell, Bath temperature N°1, Bath temperature N°2, and Bath temperature N°3.

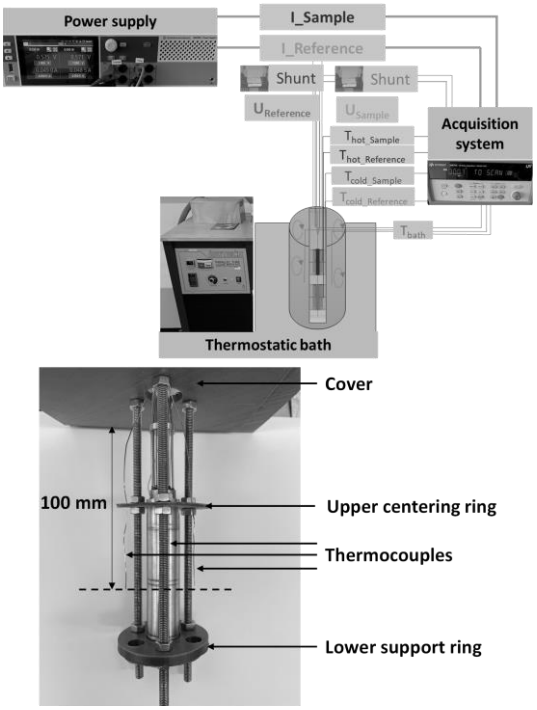

Fig. 13. A schematic representation of the new experimental set-up including photographs (upper part) and photographs of the 3-D printed calorimeter holder (lower part).

Moreover, a new calorimeter holder was developed to insert the calorimeter into the thermostatic bath. This calorimeter holder is composed of a cover, a middle ring, and a low support ring. It ensures accurate submersion, alignment, centering, and

positioning (in height and radial positions) of the calorimeter. It was made in PLA using a 3-D printer (cf. Figure 13). Three thermocouples were also inserted to measure the temperature of the fluid flow around the calorimeter at the inter-cell space level and check the temperature homogeneity of the fluid flow (100 mm above the cover).

B. The metrological characteristics of the fabricated new compact CALORRE calorimeter

Prior to the MITR irradiation, the CALORRE differential calorimeter was immersed in the thermostatic bath and then studied for a fluid temperature of 33 °C and a Reynolds number of 1607 (consistent with PLA and previous studies [8-10]). Two operating protocols were applied to test the influence of the electrical power range on the calorimetric cell responses (and thus the calorimeter response) and on their calibration curves. For both protocols, successive values of electric current are simultaneously injected for 20 minutes into the two heating elements. For the first protocol, the same electrical power is applied simultaneously to each cell up to 6 W with an electrical current injected from 0 to around 1.7 This electrical power range corresponds to the classical range used for previous studies and in particular those for the configuration N°6. Considering the mass of the head of the reference cell (2.85 g) and the sample cell (5.65 g), the corresponding nuclear heating rate ranges are 2.1 $W.g^{-1}$ and 1.1 $W.g^{-1}$ for the reference and sample cells, respectively.

Considering the nuclear heating rate results obtained by the MCNP calculations for sample and reference cells in the same axial position, a total power (not including the energy deposition on the jacket) of P_{Sample} = 10.86 W is deposited on the sample cell and $P_{Reference}$= 5.80 W on the reference cell.

Consequently, with this first protocol, the electrical power range in the sample cell is not sufficient to cover the maximal nuclear heating rate value expected in the MITR loop. Thus, a second protocol was applied. For this second protocol, distinct values of electrical power are injected into the two cells simultaneously. This protocol keeps the same values for the reference cell as those applied with the protocol N°1 and corresponds to an increased electrical power range for the sample cell, with an electrical current injected from 0 to 2.27 A and so up to 12 W. In this case, the nuclear heating rate range simulated by this 12 W power range is 2.1 $W.g^{-1}$ for the sample cell too.

The temporal response obtained with the second operating protocol is shown in Figure 14. The mean fluid flow temperature was calculated over the test duration thanks to the three thermocouples and shows good homogeneity with a temperature of 32.8 °C and a standard deviation of 0.05 °C.

The average response times (at 3τ) from 0 to 6 W for both cells with the protocol N°1 are 211 s and 191 s for the sample and reference cells respectively. The average response times (at 3τ) from 0 to 6 W for the reference cell and 12 W for the sample cell with the protocol N°2 are 208 s and 201 s respectively. This new compact calorimeter has a higher response time than that of the configuration N°6 due to its sample in stainless steel but a lower response time than that of the CALORRE differential calorimeter qualified in the MARIA reactor (equal to 291 s under the same applied laboratory conditions) due to its size [5,6]. The decrease in the response time of this new compact calorimeter is an advantage to conduct experiments in reactor. It is essential to take this response time into account during reactor experiments in order to implement or adapt the standard operating protocol.

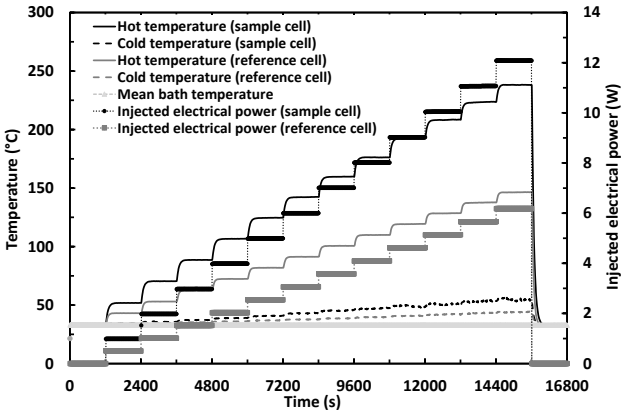

Fig. 14. Temperatures and injected electrical powers versus time for the sample and reference cells, a fluid temperature of 33 °C and a Reynolds number of 1607 obtained with the second operating protocol.

By analyzing the temporal response, the absolute temperatures can be examined, and the response time of the sensor evaluated. The maximum steady hot and cold temperatures obtained for the two operating protocols are shown in Table III. As expected, the injected electrical power ranges modify the absolute hot and cold temperatures reached in the sample cell (for the hot temperature: 148.3 °C at 6 W against 238.1 °C at 12 W). However, the influence of the injected electrical power range in the sample cell does not significantly impact the absolute hot and cold temperatures reached in the reference cell due to the lower location of this latter in the calorimeter (145.4 °C and 146.4 °C for the hot temperature for 6 and 12 W injected in the sample cell respectively). Thanks to these results, the negligible influence of the sample cell on the reference cell was demonstrated.

TABLE III
ABSOLUTE HOT AND COLD TEMPERATURES OBTAINED WITH THE TWO OPERATING PROTOCOLS

Operating protocol (-)	Calorimetric cell (-)	Injected electrical power (W)	Hot temperature (°C)	Cold temperature (°C)
N°1	Sample	6	148.3	43.3
	Reference	6	145.4	43.4
N°2	Sample	12	238.1	55.1
	Reference	6	146.4	44.2

If these results for the protocol N°1 are compared to those obtained with the individual mounting of the configuration N°6, the calorimetric cell behavior and response are quite similar (157 °C and 55.5 °C for the hot and cold temperatures, for an injected electrical power of 6 W). The difference obtained in absolute temperatures can be explained by the different envelopes and consequently, the removal of contact thermal resistances thanks to this new configuration with an increased vertical-fin.

Finally, the calibration curve of each cell, which represents the difference of the mean steady temperatures ($T_{hot} - T_{cold}$) versus the mean electrical power, is obtained by analyzing the steady states. Figure 15 shows the calibration curves obtained for the two different operating protocols. The calibration curves obtained for both operating protocols and calorimetric cells are non-linear. The calibration curve coefficients of the sample cell and the reference cell for the two operating protocols are detailed in Table IV.

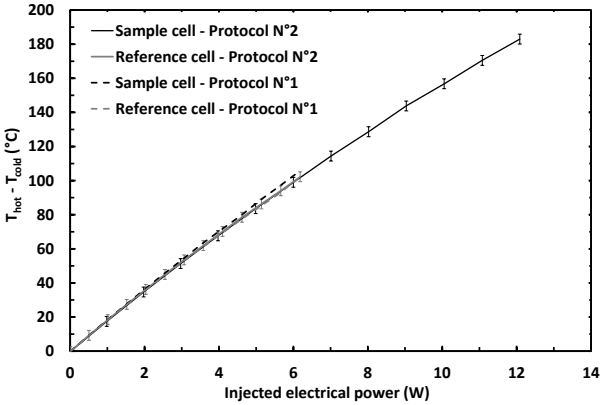

Fig. 15. Calibration curves of the sample and the reference cells obtained by applying two protocols for a fluid temperature of 33 °C and a Reynolds number of 1607.

Then, the sensitivity of each cell is calculated thanks to the calibration coefficients obtained. The sensitivity of the sample cell is equal to 15.66 °C.W^{-1} at 6 W and 12.41 °C.W^{-1} at 12 W for the operating protocols N°1 and N°2 respectively as against 14.70 °C.W^{-1} at 6 W and 14.72 °C.W^{-1} at 6 W for the reference cell. A good agreement for the sensitivity of the configuration N°6 obtained for the operating protocol N°1 at 6W is observed (15.1 °C.W^{-1}).The influence of the electrical power range is significant on the calibration curve of the sample cell.

TABLE IV
CALIBRATION CURVE COEFFICIENTS OF THE SAMPLE AND THE REFERENCE CELLS OBTAINED WITH THE TWO OPERATING PROTOCOLS

Operating protocol (-)	Calorimetric cell (-)	1st order calibration coefficient (°C.W^{-1})	2nd order calibration coefficient (°C.W^{-2})
N°1	Sample	18.54	-0.24
	Reference	18.18	-0.29
N°2	Sample	17.93	-0.23
	Reference	18.44	-0.31

The decrease in sensitivity of the sample cell demonstrates that the calorimetric cells have to be calibrated and studied on the right range of injected electrical power, simulating, therefore, the correct range of nuclear heating rate expected in a reactor.

In addition, MCNP calculation results show that the energy deposition in the reference cell is greater than in the sample cell. As this energy deposition in the reference cell structure (without sample) is higher than that in the sample cell, a correction will be necessary to determine the energy deposition in the sample which will be obtained by doing the difference of total energy deposition inside the sample cell with the corrected one inside the reference cell. For example, for an identical axial position, an energy deposition of 1.895 W.g^{-1} is obtained for the reference cell compared with 1.870 W.g^{-1} for the sample cell. This results in an energy deposition difference of +1.2%. This value should therefore be used to correct the power balance results. Moreover, during calibrations prior to the irradiation, more power should be deposited in proportion (1.2 %) in the reference cell.

V. CONCLUSION AND OUTLOOKS

The work and results presented in this article are exclusively related to the new compact CALORRE differential calorimeter fabricated thanks to prior 3-D numerical thermal parametrical results detailed in [6], in order to realize an irradiation campaign in the MITR water loop.

By considering this new compact prototype, MCNP simulations were conducted to determine the total nuclear heating rates in all components (heaters, calorimetric cell structures, sample, envelope, nose, and watertight passage) of the differential calorimeter and for 10 axial positions inside the MITR water loop. Then, using these nuclear heating rate values depending on the axial position, local heat sources were calculated and applied for numerical thermal simulations using a validated model. The calorimeter prototype was numerically studied under irradiation conditions for a heat transfer coefficient of 10000 W.m^{-2}.K^{-1} and a coolant fluid temperature of 50 °C. Experimental thermal properties as a function of temperature (up to 400 °C), for stainless steel 316L samples from the batch used for the calorimeter fabrication, were used. Thanks to this 3-D numerical study, the maximum temperatures reached within the calorimeter and on its outer wall were determined. A right behavior was observed with a maximum sensor temperature and a temperature of the external surface of its envelope respectively equal to 297.5 °C and 59.5 °C for the nuclear heating rate peak. Then, the 3-D numerical response of the sample cell and the reference cell were established as a function of the 10 axial positions of the nose cone. Finally, the response of the differential calorimeter was deduced as a function of the distance to the core center line. The results validate the feasibility of characterizing the B3 channel entirely. A relatively steady range was identified between -10 cm and -15 cm from the core centerline to perform measurements with and without displacement.

Next, the fabricated calorimeter was characterized under laboratory conditions by means of an updated experimental set-up. The key metrological characteristics of the sensor were presented (maximum temperatures, time responses, calibration curves, and sensitivities) for two different operating protocols and compared to previous calorimetric cells. These results demonstrate the importance of calibration under laboratory conditions and with the correct range of injected electrical power, especially in the case of non-linear responses. These works highlight the comprehensive approach followed to carry out online nuclear heating rate measurements inside the MITR: neutron and photon calculation with MCNP code for the new fabricated calorimeter, the measurement of thermal properties as a function of the temperature of the calorimeter structure material, 3-D thermal modeling under irradiation conditions of the calorimeter to predict its thermal response, and

experimental characterization of the calorimeter under laboratory conditions to calibrate it.

The first outlook of this work will be new MCNP calculations to determine the delayed gamma contribution and new 3-D thermal simulations of the future irradiation device under design which will be used in the MITR loop. This irradiation device will include the CALORRE calorimeter and another commercial calorimeter (gamma thermometer) to do comparison and a thermocouple). The second outlook will be the definition of the experimental protocol to be followed during the irradiation campaign based on these results already obtained: axial position, number of displacements, reactor power, fluid temperature, reproducibility testing, measurement method, etc.

ACKNOWLEDGMENT

This research work was made possible thanks to the LIMMEX joint laboratory and the IM2NP micro-mechanics workshop.

FOOTNOTES

Regarding section III.A, and specifically Figure 5, Adrien Volte created the mechanical plans (CAD drawing), and Sara Hauptman generated the geometries for the MCNP calculations based on the provided mechanical plans.

REFERENCES

[1] A. Lyoussi, D. Fourmentel, J-F. Villard, J-Y. Malo, P.Guimbal, H. Carcreff, C. Gonnier, G. Bignan, J-P. Chauvin, C. Reynard-Carette, J. Brun, O. Merroun, M. Carette, M. Muraglia, A. Janulyte, Y. Zerega and J. Andre, “Advanced methodology and instrumentation for accurate on line measurements of neutron, photon and nuclear heating parameters inside Jules Horowitz MTR Reactor”, Proceedings of Conferences RRFM and IGORR 2012, pp. 21-25, Prague, Czech Republic, 18-22 March 2012.

[2] G. Bignan, X. Bravo and P.M. Lemoine, “The Jules Horowitz Reactor: A new high Performances European MTR (Material Testing Reactor) with modern experimental capacities: Toward an International Centre of Excellence”, Proceedings of Conferences RRFM and IGORR 2012, pp. 21-25, Prague, Czech Republic, 18-22 March 2012.

[3] H. Carcreff, L. Salmon and F. Malouch, “Recent developments in nuclear heating measurement methods inside the OSIRIS reactor”, Nucl. Instrum. Methods Phys. Res. A, Accel. Spectrom. Detect. Assoc. Equip., vol. 942, pp. 1-19, Oct. 2019.

[4] H. Carcreff, V. Radulovic, D. Fourmentel, K. Ambrozic, C. Destouches, L. Snoj and N. Thiollay, “Nuclear heating measurements for fusion and fission relevant materials in the JSI TRIGA reactor”, Fusion Eng. Des. 179 (2022), 113136.

[5] M. Carette, A. Lyoussi, J. Brun, C. Reynard-Carette, J.F. Villard, « Eprouvette pour mesure d'échauffements nucléaire dans un réacteur nucléaire, et cellule calorimétrique comprenant au moins une telle éprouvette », FR1553136A, 2015-04-10.

[6] M. Carette, A. Lyoussi, J. Brun, C. Reynard-Carette, J.F. Villard, P. Guimbal, “Sample holder for measuring nuclear heating in a nuclear reactor, and calorimetric cell including at least one such sample holder”, CEA/AMU, US patent, US10755823B2, 2020-08-25.

[7] C. Reynard-Carette, G. Kohse, J. Brun, M. Carette, A. Volte, A. Lyoussi, "Review of nuclear heating measurement by calorimetry in France and USA", Proc. ANIMMA 2017, Jun. 2017, EPJ Web of Conferences 170, 04019 (2018).

[8] A.Volte, C. Reynard-Carette, A. Lyoussi, J. Brun, M. Carette, "Study of the Response of a New Compact Calorimetric Cell for Nuclear Heating Rate Measurements", IEEE Trans. Nucl. Sci., vol. 65, no. 9, pp. 2461-2470, Sept. 2018, doi: 10.1109/TNS.2018.2827084.

[9] A.Volte, J. Brun, A. Lyoussi, M. Carette, C. Reynard-Carette, “Qualification of a New Differential Calorimeter Configuration Dedicated to Nuclear Heating Rates up to 20 W.g-1”, IEEE Trans. Nucl. Sci., vol. 67, no. 11, pp. 2405-2414, Nov. 2020, doi: 10.1109/TNS.2020.3027913.

[10] A.Volte, M. Carette, A. Lyoussi, G. Kohse, J. Rebaud, V. Valero, C. Reynard-Carette, “Review of CALORRE Calorimeter Characterizations Under Laboratory and Irradiation Conditions”, IEEE Trans. Nucl. Sci., vol. 69, no. 4, pp. 840-848, April 2022, doi: 10.1109/TNS.2022.3150148.

[11] S. Hauptman, A. Volte, G. Kohse, M. Carette, C. Reynard-Carette, “Flux and Nuclear Heating Rate Calculations for CALORRE Irradiation in MITR”, ANIMMA conference, Lucca, Italy, 2023.

[12] MIT Research Reactor, http://nrl.mit.edu/reactor (2023)

[13] MIT Nuclear Reactor Laboratory, “In-Core Experiments,” Facilities, https://nrl.mit.edu/facilities/in-core (accessed July, 2023).

[14] X-5 Monte Carlo Team, MCNP – A General Monte Carlo N-Particle Transport Code, Version 5, Volume II: User’s Guide. April 24, 2003.

[15] M.B. Chadwick, P. Obložinský, M. Herman, N.M. Greene, R.D. McKnight, D.L. Smith, P.G. Young, R.E. MacFarlane, G.M. Hale, S.C. Frankle, A.C. Kahler, T. Kawano, R.C. Little, D.G. Madland, P. Moller, R.D. Mosteller, P.R. Page, P. Talou, H. Trellue, M.C. White, W.B. Wilson, R. Arcilla, C.L. Dunford, S.F. Mughabghab, B. Pritychenko, D. Rochman, A.A. Sonzogni, C.R. Lubitz, T.H. Trumbull, J.P. Weinman, D.A. Brown, D.E. Cullen, D.P. Heinrichs, D.P. McNabb, H. Derrien, M.E. Dunn, N.M. Larson, L.C. Leal, A.D. Carlson, R.C. Block, J.B. Briggs, E.T. Cheng, H.C. Huria, M.L. Zerkle, K.S. Kozier, A. Courcelle, V. Pronyaev, S.C. van der Marck, "ENDF/B-VII.0: Next generation evaluated nuclear data library for nuclear science and technology", Nucl. Data Sheets 107(2006)2931.

[16] H. Amharrak, C. Reynard-Carette, A. Lyoussi, M. Carette, J.Brun, C. DeVita, D. Fourmentel, and J-F. Villard, “Parametric study of the energy deposition inside the calorimeter measuring the nuclear heating in Material Testing Reactors”, Nuclear Instruments and Methods in Physics Research A 799, 17–24 (2015)

[17] R. Van Nieuwenhove and L. Vermeeren, "Nuclear Heating Measurements by Gamma and Neutron Thermometers," IEEE Trans. Nucl. Sci., vol. 67, no. 9, pp. 2073-2080, Sept. 2020, doi: 10.1109/TNS.2020.2984782.

[18] M. Lemaire, “Validation des calculs d’échauffements photoniques en réacteur d’irradiation au moyen du programme expérimental AMMON et du dispositif CARMEN.", PhD manuscript, 2015.

[19] A. Peron, “Contribution à l'amélioration des méthodes d'évaluation de l'échauffement nucléaire dans les réacteurs nucléaires à l'aide du code Monte-Carlo TRIPOLI-4", PhD manuscript, 2015.

[20] K. Sun, “Nuclear Heating Rate of Bounding Case FS-2 Design” Internal MIT Nuclear Reactor Laboratory Document. April 2014.